

10  
2-4-92 JSD

## CONTRACTOR REPORT

SAND87-7082  
Unlimited Release  
UC-814

### Yucca Mountain Site Characterization Project

# Effects of a Potential Drop of a Shipping Cask, a Waste Container, and a Bare Fuel Assembly During Waste-Handling Operations

C. L. Wu, J. Lee, D. L. Wu, L. J. Jardine  
Bechtel National, Inc.  
50 Beale Street  
San Francisco, CA 94105

Prepared by Sandia National Laboratories Albuquerque, New Mexico 87185  
and Livermore, California 94550 for the United States Department of Energy  
under Contract DE-AC04-76DP00789

Printed December 1991

DISTRIBUTION OF THIS DOCUMENT IS UNLIMITED

SAND--87-7082

DE92 006828

Distribution  
Category UC-814

SAND87-7082  
Unlimited Release  
Printed December 1991

EFFECTS OF A POTENTIAL DROP OF A SHIPPING CASK, A WASTE CONTAINER,  
AND A BARE FUEL ASSEMBLY DURING  
WASTE-HANDLING OPERATIONS

by

C. L. Wu, J. Lee, D. L. Wu, L. J. Jardine

Bechtel National, Inc.  
50 Beale Street  
San Francisco, CA 94105

for

Sandia National Laboratories  
P.O. Box 5800  
Albuquerque, NM 87185

Under Sandia Contract: 52-9817

Sandia Contract Monitor  
C. V. Subramanian  
Principal Investigator  
C. V. Subramanian  
Nuclear Waste Engineering Projects Division

ABSTRACT

This study investigates the effects of potential drops of a typical shipping cask, waste container, and bare fuel assembly during waste-handling operations at the prospective Yucca Mountain Repository. The waste-handling process (one stage, no consolidation configuration) is examined to estimate the maximum loads imposed on typical casks and containers as they are handled by various pieces of equipment during waste-handling operations. Maximum potential drop heights for casks and containers are also evaluated for different operations.

A nonlinear finite-element model is employed to represent a hybrid spent fuel container subject to drop heights of up to 30 ft onto a reinforced concrete floor. The impact stress, strain, and deformation are calculated, and compared to the failure criteria to estimate the limiting (maximum permissible) drop height for the waste container. A typical Westinghouse 17 x 17 FW fuel assembly is analyzed by a simplified model to estimate the energy absorption by various parts of the fuel assembly during a 30 ft drop, and to determine the amount of kinetic energy in a fuel pin at impact. A nonlinear finite-element analysis of an individual fuel pin is also performed to estimate the amount of fuel pellet fracture due to impact.

This work was completed on May 1990.

MASTER

DISTRIBUTION OF THIS DOCUMENT IS UNLIMITED

## EXECUTIVE SUMMARY

### Scope

This study investigates the effects of potential drops of a typical shipping cask, a waste container, a bare fuel assembly, and an individual fuel pin during the waste-handling operations at the potential Yucca Mountain repository.

The waste-handling process for the waste-handling building (one stage, no consolidation configuration) is examined. Several waste-handling scenarios involving cask and container impacts are described, estimates are made of the maximum loads imposed on different parts of a cask or container, and methods of mitigating the effects of these impacts are discussed.

Impact analyses are performed to estimate the limiting drop height of a waste container (the maximum height it can fall without unacceptable damage) and to assess the potential damage to a bare fuel assembly/individual fuel pin in the event of an assembly/pin drop. For the case of a spent fuel assembly, the mechanism of fuel pellet pulverization is discussed.

### Cask and Container Drops During Waste-Handling Operations

For a shipping cask, the following cases were considered: toppling, rolling off a cask transfer car and landing in a horizontal position on the floor, swinging against a wall or a 2 in. dia. object, and falling 2 ft. The results of these load envelope studies indicate that maximum stresses occur when the cask rolls off a transfer car and strikes the floor. These maximum (compressive) stresses are about 21,000 psi and 19,000 psi for a truck cask and a rail cask, respectively. Because these stresses do not exceed the allowable stress\* (21,000 psi) for 304L stainless steel, neither truck cask nor rail cask should fail.

---

\* The allowable compressive stress is taken to be 60 percent of the yield stress.

For an empty container, the following cases were considered: dead load, ovaling due to stacking, swinging like a pendulum, impacting the hot-cell walls, impact between containers, swinging against a stationary 2 in. dia. and 1 ft dia. object, and striking a concrete floor after free-falling 2 ft or 34 ft. The results of this load envelope study indicate that the maximum stresses occur as a consequence of a free fall from the maximum drop height of 34 ft or of an impact on the hot-cell walls. These stresses are about 26,000 psi (compressive) and 22,000 psi (bending). The bending stress is less than the allowable stress (23,000 psi) for 304L stainless steel; the compressive stress is slightly greater than the allowable stress (21,000 psi) for 304L stainless steel, but will not result in a fracture of the container.

For a loaded container, the following cases were considered: dead load; swinging like a pendulum; impacting the hot-cell walls; swinging against a stationary 0.2 in. dia. or 6 in. dia. object; free-falling 2 ft onto the floor, a 6 in. dia. object, or a 2 in. dia. object; and seismic loads. The results of the load envelope study indicate that the maximum stress occurs when the container impacts the hot-cell walls or a 2 in. dia. stationary object. The value of this stress is about 81,000 psi (bending), which is almost four times as great as the allowable stress for 304L stainless steel, but not great enough to result in a fracture. (The ultimate strength of this material is 85,000 psi, and the critical fracture strength is 228,000 psi.)

There are several ways of mitigating the effects of a potential drop. These mitigation techniques, which are based on the load analysis and potential drop heights, include equipment rearrangement, structural modifications, and the use of energy-absorbing materials.

#### Determining the Limiting Drop Height of a Loaded Container

Investigations were carried out to determine a loaded (spent fuel) waste container's limiting drop height, defined as the maximum vertical distance the container can fall without being shortened through impact by more than 1.0 in. and without undergoing an effective plastic strain greater than 0.15. A literature search was conducted to collect

published information. Next, three finite-element impact analyses using the computer program, DYNA3D, were performed for drop heights of 30 ft, 7.5 ft, and 5.0 ft. The results of these analyses were compared with the results of experimental tests, described in the literature, involving a 30 ft drop of defense high-level waste (DHLW) canisters. It was found that:

- o The results of the DYNA3D analysis for a 30 ft drop of a loaded spent fuel container agree with those of the experimental drop tests for a DHLW canister.
- o The limiting drop height of a loaded spent fuel container is about 3.8 ft.

To obtain a more detailed analysis, future studies of the effects of impact on a loaded spent fuel or DHLW waste container are recommended. These studies should cover:

- o The effect of container impact orientation, especially impacts directly on the pintle of the container
- o The effect of total container weight on the limiting drop height
- o The effect on the limiting drop height of (1) interactions between the fuel assemblies and (2) interactions between the fuel assemblies and the container
- o The effects of impacts on sharp objects and for various target conditions

#### Analysis of an Accidental Drop of a Typical Bare Fuel Assembly or of an Individual Fuel Pin

The analysis of an accidental drop of a fuel assembly or a fuel pin proceeded as follows: (1) a literature search was performed; (2) hand calculations were carried out to estimate the energy absorption by the various parts and fuel pins of a fuel assembly; and (3) a finite-element

impact analysis was conducted by employing the computer program, DYNA3D, for an individual fuel pin within a fuel assembly. In both the hand calculations and the finite-element analysis, a 30 ft drop was assumed.

As a result of these studies, the following conclusions were drawn:

- o The friction between fuel pins and the grid spacers dissipates only a small amount of the impact energy, approximately equal to 3 percent of the total kinetic energy imparted to the fuel pins.
- o The bottom 1.3 in. of fuel pellets (which is less than 1 percent of the total volume) fractures.
- o The zircaloy cladding fails in the region where the fractured fuel pellet bulges out radially (0.15 to 0.45 in. from the bottom of the fuel pellet).
- o There is no failure in the bottom end plug of the fuel pin.

Further studies on the effect of impacts on fuel assemblies and fuel pins are recommended. These studies should investigate the effect of buckling on the failure of fuel pellets and the zircaloy cladding. A simplified finite-element model can be created for the fuel assembly and its numerous fuel pins. Instead of performing a hand calculation using the energy balance method, one can conduct a finite-element impact analysis of the entire fuel assembly to determine the energy absorption of the bottom nozzle. In this way, the effect of the bottom nozzle on the dynamic response of fuel pins can be accounted for more realistically. The effects of nonperpendicular impact and of impacts on various target conditions should also be investigated.

#### Fuel Pellet Pulverization

The studies on fuel pellet pulverization performed by Argonne National Laboratory were reviewed. These studies included a series of drop-weight impact tests of representative materials such as pyrex glass, Macor glass ceramic, and sintered UO<sub>2</sub> ceramic.

Page 5-3

All results showed that the fracture particulate proper, which included all particles of respirable size (i.e., diameters less than 10 microns), and which contained more than about 90 percent of the total surface area, had a straight-line size distribution when plotted on lognormal graphical coordinates.

It was found the volume fraction of particles with diameters less than 10 microns is directly proportional to input energy density. No significant difference between axial and diametrical impact was found.

Further studies are recommended which examine and develop the relationships and possible correlations between the laboratory-scale results on small specimens and the finite-element analysis results for a single full-scale spent fuel rod.

#### 4.0 ANALYSIS OF AN ACCIDENTAL DROP OF A TYPICAL BARE FUEL ASSEMBLY OR OF AN INDIVIDUAL FUEL PIN

In this section, the accidental drop of a bare nuclear fuel assembly is analyzed and an impact analysis of fuel pins and fuel pellets is performed. The Westinghouse 17 x 17 PWR fuel assembly was selected for the fuel assembly drop analysis. This is typical of the spent fuel assemblies to be received at the repository.

This section consists of the following subsections:

- o Subsection 4.1. Assumptions
- o Subsection 4.2. Literature Search
- o Subsection 4.3. Estimate of Energy Absorption by Various Parts of the Fuel Assembly
- o Subsection 4.4. Effect of Impact on Fuel Pins and Fuel Pellets

#### 4.1 Assumptions

- o The ceramic spent fuel pellets are characterized by their brittle fracture behavior. The brittle fracture occurs when the strain exceeds 1.1 times the yield strain of the ceramic fuel material.\*
- o The zircaloy cladding of the fuel pin is characterized by its elastic-plastic fracture behavior. The fracture failure of the zircaloy occurs when the strain exceeds 9 percent.\*

#### 4.2 Literature Search

##### 4.2.1 Introduction

The purpose of this task is to determine, using simplified but rigorous analytical techniques, the consequences of an accidental

---

\* See Subsection 4.4.4 for details.

drop of (1) a bare fuel assembly or (2) a fuel pin. The task was initiated by a literature search to collect recent technical information on:

- o Research literature related to the drop of fuel assemblies
- o Geometrical and mechanical properties of a typical fuel assembly
- o Mechanical properties of fuel tube cladding material in the irradiated state
- o Analytical techniques for impact analyses

Most of the technical literature defining impact loads is concerned with the target rather than the projectile, thus greatly restricting the available resources. The major fuel assembly vendors (Westinghouse, Combustion Engineering, Babcock and Wilcox) have conducted in-house impact analyses for each of their (or their clients') assemblies. Unfortunately, most of the data and the results are proprietary and could not be obtained. Because the literature data base is so limited, the search was expanded to include impact analyses of other types of equipment. A representative example is the Reactor Vessel Head Drop analysis by Westinghouse (Ref. 16), which uses a simplified method to describe the impact load (outlined by Koark in Ref. 17). The procedure and assumptions described therein are employed to a large extent in the simplified analysis of the fuel assembly.

Possible modes of failure for various components of a fuel assembly were determined after compilation and assessment of industry-wide experience with fuel assembly damage caused by abnormal conditions in handling and transporting operations. Much of this information, which is summarized in detail in Ref. 18, is found in its entirety in the U.S. NRC's Public Document Room. As of 1982, 34 fuel assemblies have been dropped during handling operations. All the drops were in water, some with nondirect impacts. Therefore, these cases have less serious consequences

than a drop through air. Typical examples of the damage sustained by BWR and PWR fuel rods and bundles include:

- o Spacer grid damaged
- o Lower tie plate damaged
- o Assembly skeleton/wrapper/can twisted, bowed, or distorted
- o Channel spacers bent or disturbed
- o Channel deformed
- o Fuel pin bent, bowed, lost, dropped, difficult to remove, or broken
- o Upper nozzle broken off assembly or damaged
- o Lower nozzle damaged
- o Nozzle springs bent or broken
- o Nut capture devices bent

Damage to fuel assemblies and fuel pins as a result of handling is generally detected by visual techniques (direct observation, binoculars, periscope, or closed-circuit television). Fuel assemblies having fuel pins with breached cladding can be detected by gas release, radiation monitoring, or leak-testing (sipping). Damage to fuel pins can also be detected by eddy-current and ultrasonic techniques.

#### 4.2.2 Summary of Recent Fuel Damage Experiences

Additional case histories of fuel assembly drops are available in Abnormal Occurrence Reports submitted to NRC by utility companies. Reports collected from several nuclear power generating stations describe a variety of fuel assembly drops on several surfaces and at different orientations. Damage to the assemblies varied widely, as indicated below.

##### 4.2.2.1 Example 1

During transfer of fuel from the core to a fuel storage pool, one fuel assembly was inadvertently dropped 9.1 m (30 ft) onto another

fuel assembly in the core. The lower tie plate cage on the first assembly was deformed upwards toward the tie plate. The ball handle on the second was deformed almost horizontally; the channel was driven downward so that its lower edge flared over the lower tie plate shoulder. Movement of the second assembly caused a tensile force to be applied to the fuel pins, and during this movement, there was a temporary increase in airborne radioactivity, which apparently indicated that the fuel pins had been damaged to some extent. Channels on two fuel assemblies that were adjacent to the second assembly were dented on the top edge.

BWR

#### 4.2.2.2 Example 2

During unloading of the core, a channeled fuel assembly came loose from the grapple and dropped about 3.7 m (12 ft) to the transfer pool floor. No gaseous release was noted, and there was no apparent damage to the fuel assembly.

BWR

#### 4.2.2.3 Example 3

During transfer, an irradiated fuel assembly became detached from the grapple and fell about 6 m (20 ft) into the spent fuel pool. The grapple hook apparently had not been completely latched under the handle of the fuel assembly. There was no measurable release of radioactivity. The nose piece and the nose piece end of the fuel channel were crushed, but there was no indication of broken fuel pins.

BWR

#### 4.2.2.4 Example 4

Because of improper grappling, an irradiated fuel assembly dropped about 1.8 m (6 ft) to the spent fuel pool floor and then tipped over into the corner of the pool in the 3 m (10 ft) deep spent fuel cank pit. When the fuel assembly was lifted to a vertical position, the channel fell off and fuel pins came out of the

BWR

assembly. Apparently, the fuel assembly separated because the tie rods and/or tie rod keepers had been sheared when the assembly hit the pool floor.

#### 4.2.2.5 Example 5

← upper?

One fuel assembly fell from the fuel preparation machine from a vertical to a horizontal position. Only three other fuel assemblies were struck or could have been struck by the falling assembly. The fuel assembly that fell was not visibly damaged; however, the bail of another fuel assembly was bent. Preliminary visual inspection of the two other assemblies indicated localized scratches or crud removal on the bails. Inspection of the fuel preparation machine indicated that the upper roller guide had separated from the carriage.

#### 4.2.2.6 Example 6

— BUR

During transfer of an unchanneled spent fuel assembly from a fuel preparation machine to a spent fuel rack in the fuel pool, the assembly fell about 1.5 m (5 ft) from the main grapple to the pool floor because of a grapple design deficiency. No release of radioactivity was measured even though the assembly was damaged. (Visual inspection of the assembly revealed it to be considerably bowed over its whole length.)

#### 4.2.2.7 Conclusion

This summary of recent fuel damage experience in underwater environments from abnormal handling and transporting operations shows that in most cases involving damage, minor degradation of fuel assembly components did not cause a breaching of the fuel pin cladding or a release of radioactive gases or solids. This was true even in those cases where the fuel assemblies fell as far as 30 ft through water and impacted other fuel assemblies or the bottom of the spent fuel storage pool.

#### 4.2.3 Geometrical and Mechanical Properties of Fuel Assemblies

Technical descriptions of the geometrical and mechanical properties of a variety of fuel assemblies were compiled to facilitate selection of a reference configuration for analytical purposes. Information was gathered for Westinghouse 14 x 14, 15 x 15, 16 x 16, and 17 x 17 PWR fuel assemblies, G.E. 7 x 7 and 8 x 8 BWR fuel assemblies, the Babcock and Wilcox 15 x 15 PWR fuel assembly, and the Combustion Engineering 15 x 15 PWR fuel assembly. All pertinent mechanical design parameters and properties are tabulated in the literature (Refs. 19, 20, 21, and 22).

It was necessary to select one of the above assemblies as the reference assembly because there is no standard design for any vendor and in-house designs are continually being modified. Many design details are considered proprietary by the fuel vendors. Some consider only the mechanical design proprietary; others consider the materials used for specific components proprietary. This further restricts the selection of a representative assembly, and makes it impossible to define the same level of detail for all the fuel bundle types. On the basis of the available information, the Westinghouse 17 x 17 design was selected.

#### 4.2.4 The Effect of Irradiation on Zirconium Alloy Cladding

The effect of fast-neutron irradiation on zirconium alloys used for the fuel tube cladding material has been documented by numerous investigators. These changes include an increase in tensile strength, a reduction in impact strength, and a decrease in ductility. The pertinent mechanical properties of irradiated zircaloy were extracted from the technical literature for use in the nonlinear fuel pin impact analysis. These properties are discussed in detail in Subsection 4.4. Most researchers agree on the principal effects of irradiation on most mechanical properties. However, there are many differences of detail, and it is clear that materials supplied by different manufacturers or fabricated differently can vary significantly in mechanical properties.

Not an  
issue for  
fresh fuel  
analysis

#### 4.3 Estimate of Energy Absorption by Various Parts of the Fuel Assembly

In the present design configuration, the bare fuel assemblies are handled in the fuel unloading hot cells. The floor level of the cask transfer tunnel, the fuel racks and other isolated areas are 25 ft below the floor elevation of the fuel unloading hot cells. Allowing 5 ft clearance for handling in the fuel unloading hot cell, the maximum potential drop height during waste-handling operations is approximately 30 ft. Hence, this analysis was conducted to estimate the amount of energy absorbed by a typical fuel assembly after an accidental drop from a height of 30 ft.

Energy balance methods were used to determine the percentage of impact energy absorbed by various parts of the fuel assembly. The analytical model used for impact analysis is an adaptation of the seismic model created by Westinghouse (Ref. 23). Since the mass, stiffness, and damping properties of this model are proprietary information, it was necessary to revise the model and recalculate the properties.

##### 4.3.1 Fuel Assembly Description

The fuel assembly selected for this study is the Westinghouse Standard 17 x 17 PWR fuel assembly, shown in Figure 4-1. The 17 x 17 design incorporates an array of 289 positions, of which 264 are occupied by fuel pins. The remaining 25 positions are occupied by 24 guide tubes and one instrument tube in which a variety of other components are inserted. Also included are upper and lower end fittings (nozzles), which are made of cast type-304 stainless steel. Eight fuel rod spacers (grid assemblies) maintain rod-to-rod configuration along the length of the assembly. These grids, as well as the rods and tubes, are made of zircaloy-4. The 24 guide tubes and the instrument tube are externally larger than the fuel pins, but replace only one fuel pin each. The physical properties of all elements in the assembly are given in Table 4-1.

Table 4-1

MECHANICAL DESIGN PARAMETERS FOR THE WESTINGHOUSE 17 x 17  
STANDARD PWR FUEL ASSEMBLY

<u>Item</u>	<u>Value</u>
<b>Assembly</b>	
Transverse dimension, in.	8.426
Assembly weight, lb	1,467
UO <sub>2</sub> /assembly, lb	1,154
Overall length, in.	159.8
<b>Fuel pins</b>	
Number per assembly	264
Length, in.	151.635
Fuel length, in.	144
OD, in.	0.374
Diametral gap, in.	0.0065
Clad thickness, in.	0.0225
Clad material	Zr-4
<b>Fuel pellets</b>	
Type	UO <sub>2</sub>
Total weight/pin, lb	4.37
<b>Guide tubes</b>	
Number/assembly	24
OD, in.	0.474
Wall thickness, in.	0.016
Material	Zr-4
<b>Instrument tube</b>	
Number/assembly	1
OD, in.	0.48
Material	Zr-4
<b>Bottom nozzle</b>	
Material	SS 304

#### 4.3.2 Analytical Model of Fuel Assembly

The fuel assembly is idealized by an assembly of masses, springs, and a gap, as shown in Figure 4-2. This model is a simplified version of the computer model used for the Westinghouse seismic study (Ref. 23). The fuel pins and fuel pellets are lumped together as a single mass which is supported (before impact) by the friction between the fuel pins and grid assemblies. This friction force is assumed to be 100 lb/tube as a reasonable average value, giving a total friction force of 26.4 kips.

The grid assemblies are supported by the guide thimbles and the instrument tube. The fuel pins are mounted on the grids so that there is a 0.75 in. gap between the fuel pins and the bottom nozzle assembly. Upon impact, the kinetic energy is initially absorbed by friction between the grid assembly and fuel pins and compression of the guide thimbles.

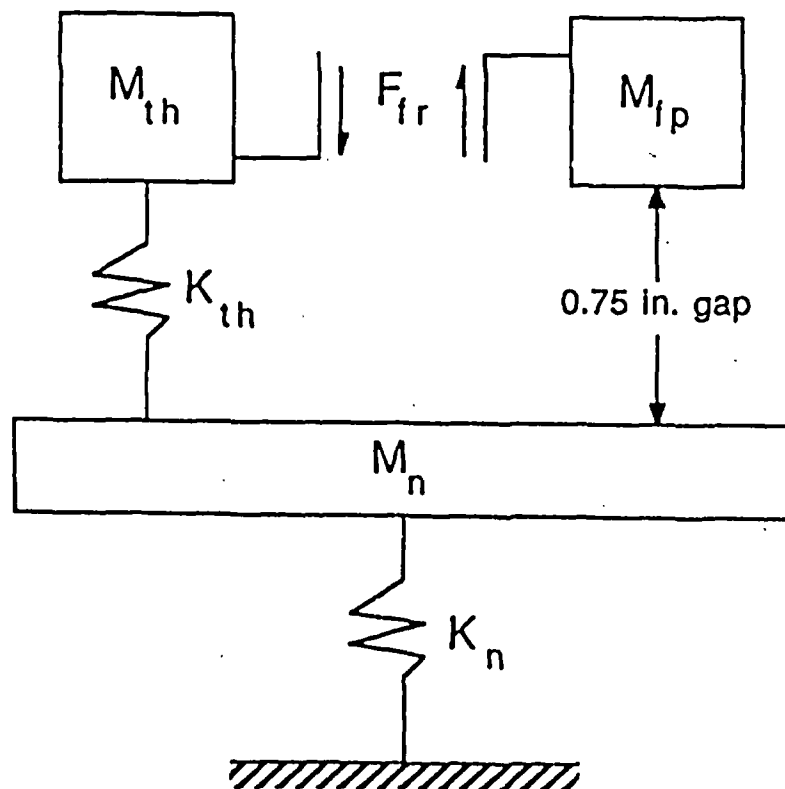
The spring constants for the fuel pins and guide tubes were determined from the equation:

$$k = \frac{nAE}{L}$$

where

- E = modulus of elasticity at temperature of 300°C
- L = one half of the length of fuel pin or guide tube
- n = number of tubes
- A = cross-sectional area of tube

Stiffness values obtained in this way are slightly higher than those computed considering the actual cross-sectional geometry. Consequently, the force required to initiate yielding of the guide tubes, computed as the product of the cross-sectional area and yield stress of the tubes, is approximately 30.9 kips.



$M_{fp}$  = Mass of fuel pins

$F_{fr}$  = Friction force between fuel pins and grid assembly

$M_{th}$  = Mass of thimbles

$K_{th}$  = Stiffness of thimbles

$M_n$  = Mass of bottom nozzle

$K_n$  = Stiffness of bottom nozzle

Figure 4-2  
Analytical Model of a Fuel Assembly

#### 4.3.2 Analytical Model of Fuel Assembly

The fuel assembly is idealized by an assembly of masses, springs, and a gap, as shown in Figure 4-2. This model is a simplified version of the computer model used for the Westinghouse seismic study (Ref. 23). The fuel pins and fuel pellets are lumped together as a single mass which is supported (before impact) by the friction between the fuel pins and grid assemblies. This friction force is assumed to be 100 lb/tube as a reasonable average value, giving a total friction force of 26.4 kips.

The grid assemblies are supported by the guide thimbles and the instrument tube. The fuel pins are mounted on the grids so that there is a 0.75 in. gap between the fuel pins and the bottom nozzle assembly. Upon impact, the kinetic energy is initially absorbed by friction between the grid assembly and fuel pins and compression of the guide thimbles.

The spring constants for the fuel pins and guide tubes were determined from the equation:

$$k = \frac{nAE}{L}$$

where

- E = modulus of elasticity at temperature of 300°C
- L = one half of the length of fuel pin or guide tube
- n = number of tubes
- A = cross-sectional area of tube

Stiffness values obtained in this way are slightly higher than those computed considering the actual cross-sectional geometry. Consequently, the force required to initiate yielding of the guide tubes, computed as the product of the cross-sectional area and yield stress of the tubes, is approximately 30.9 kips.

Once fuel pins have impacted the bottom nozzle, the kinetic energy is absorbed by compression of both the guide thimbles and the fuel pins as well as the friction resistance. In addition, the bottom nozzle absorbs kinetic energy through flexural deformation of the bottom plate and compression of the nozzle legs.

#### 4.3.3 Loading Condition

A conservative estimate of the load is made by assuming that the impact occurs vertically on a rigid surface and that the fuel assembly does not rebound. Consequently, the total energy imparted to the model is equal to the kinetic energy of the fuel assembly after it has fallen 30 ft. The velocity,  $v$ , upon impact is

$$\begin{aligned}v &= (2 gh)^{1/2} \\ &= 44 \text{ fps}\end{aligned}$$

The total mass is 45.6 lb-sec<sup>2</sup>/ft. Thus, the total impact energy, KE, for the fuel assembly is

$$\begin{aligned}KE &= 1/2 mv^2 \\ &= 44,100 \text{ ft-lb, or } 530 \text{ k-in.}\end{aligned}$$

#### 4.3.4 Analytical Results

Energy dissipation by several modes of failure of fuel assembly components were examined. These include friction between the grid assembly and fuel rod, compression of the guide tubes, compression of the fuel rods, bending of the bottom nozzle base plate, and compression of the bottom nozzle legs.

The amount of energy dissipated as strain energy in each component of the fuel assembly is computed from the force-displacement curves for each. The friction mechanism and the spring representing the guide tube stiffness in the model act in series.

Since the maximum friction force is lower than the yield force of the guide tubes, the frictional resistance is overcome first. The energy required to close the 0.75 in. gap between the bottom nozzle and the fuel pin is 14 k-in. This is the sum of the energy dissipated by the friction between the fuel pins and the thimbles and the elastic strain energy resulting from the compression of the thimbles and instrument tubes. This 14 k-in. energy is about 3 percent of the total energy imparted to the fuel pins. At the moment when the fuel pins have just impacted the bottom nozzle, the guide tubes have not yet been stressed to yield, and the kinetic energy of fuel pins is 516 k-in. This energy is absorbed in the deformation of the fuel pins.

In the above calculation, it is assumed that the bottom nozzle is infinitely rigid. This nozzle, however, could be included in the model with a stiffness equal to the flexural stiffness of a 6.75 in. x 6.75 in. square plate, simply supported at the four nozzle legs, subjected to a uniform load. Since the information about the nozzle leg was not completely available, the actual stiffness and the yield force of the bottom nozzle could not be readily calculated. Judging from the pictorial representation of the nozzle, it was believed that this force is much larger than the friction force between the fuel pins and the grid assembly, in which case the previous rigid nozzle assumption would still be valid. The key question concerns the pin-nozzle interaction, namely, How much kinetic energy is absorbed by the fuel pins and how much by the bottom nozzle after the fuel pins have impacted the bottom nozzle? The effect of the bottom nozzle on the maximum stress and strain of the fuel pins can be calculated only when more information about the bottom nozzle becomes available.

#### 4.3.5 Conclusion and Recommendations

Based on the rigid bottom nozzle assumption, when a standard Westinghouse 17 x 17 fuel assembly is dropped from a height of 30 ft, 483 k-in. of kinetic energy is retained in the fuel pins after they have impacted the bottom nozzle. This constitutes 97 percent of the initial energy imparted to the fuel pins. Further refinements of the model and finite-element techniques are needed to account for the effect of the bottom nozzle on the dynamic response of fuel pins during the pin-nozzle interaction.

#### 4.4 Effect of Impact on Fuel Pins and Fuel Pellets

##### 4.4.1 Assumptions Used in the Impact Analysis

The typical fuel pin structure of a standard Westinghouse 17 x 17 fuel assembly is shown in Figure 4-3. An impact analysis of the fuel pin was performed using the finite-element computer program DYNA3D. Only axisymmetrical deformation was considered; no lateral buckling deformation was investigated. The following assumptions were made:

- o A separated individual fuel pin is dropped 30 ft in a vertical position and strikes a rigid target surface in a perpendicular direction.
- o Fuel pellets are rigidly connected as a continuous piece of cylinder.

##### 4.4.2 Finite-Element Model of a Fuel Pin

As assumed previously, the deformation of fuel pins after impact would be axisymmetrical. A three-dimensional model for a quarter fuel pin was created. The model consists of 5,202 solid elements and 12,424 nodal points. Among these elements, 2,160 elements were employed to model fuel pellets, and 3,000 to model zircaloy cladding. Top and bottom end plugs were also modeled.

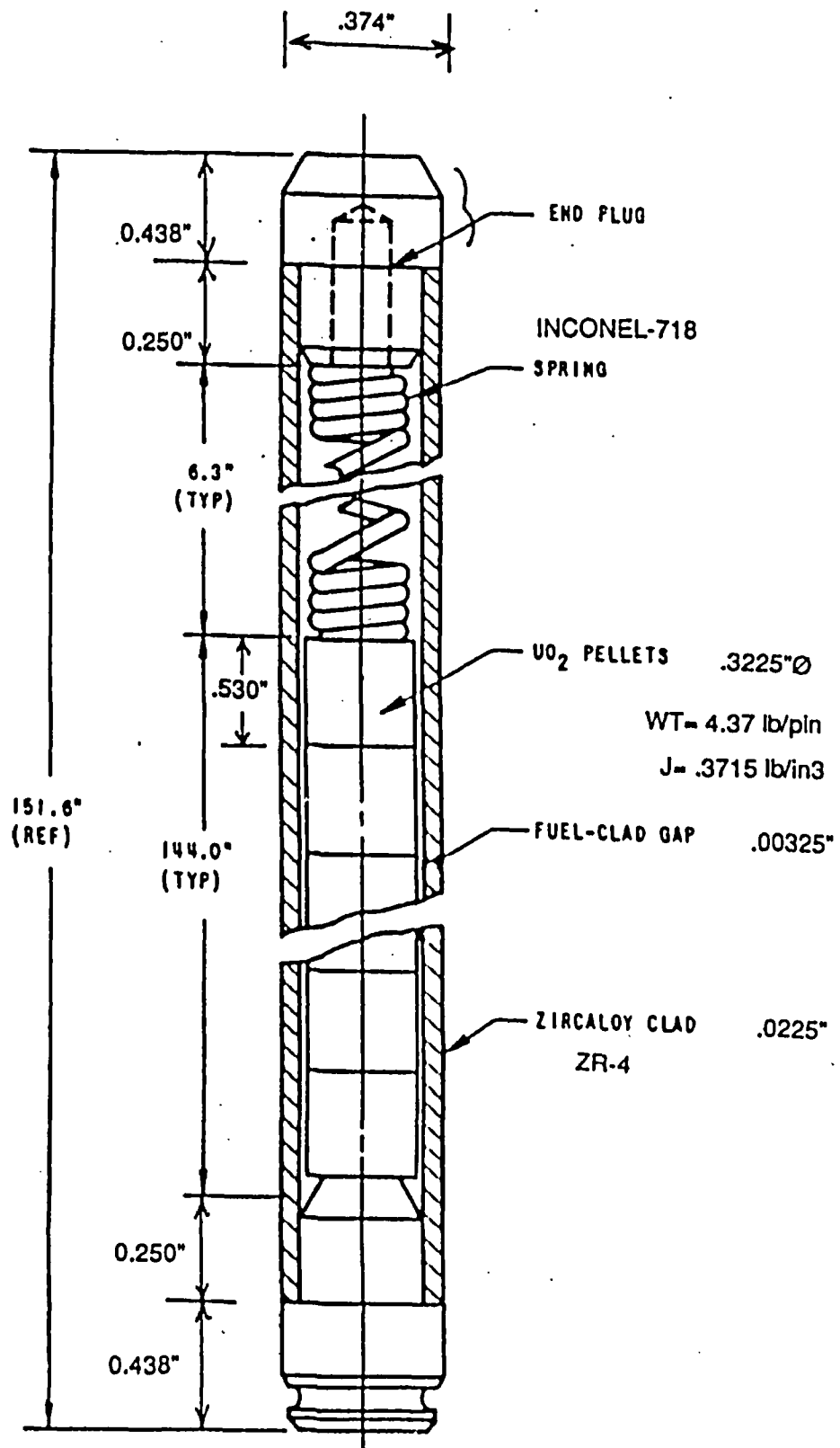


Figure 4-3  
 Fuel Pin Structure.

The spring inside the fuel pin was not considered in the model because the initial spring force on fuel pellets would be reduced rather than increased before the fuel pellets started to rebound.

Every nodal point in this model is completely free, except that those lying in the symmetrical planes are constrained in the direction normal to the plane. Figures 4-4, 4-5, 4-6, and 4-7 show a typical section for each component in this model; Table 4-2 summarizes the nodal point and element ranges for these components.

In this model, three sliding interface surfaces are defined. The first interface surface defines the contact between the bottom surface of the bottom end plug and the rigid target plate; the second interface describes the interaction between the bottom surface of fuel pellets and the top surface of the bottom end plug; and the third interface defines the interaction between the inner cylindrical surface of zircaloy cladding and fuel pellets. All of these three interfaces allow contact surfaces to slide against one another with gaps.

Table 4-2

## SUMMARY OF THE FINITE-ELEMENT MODEL OF THE FUEL PIN

<u>Component</u>	<u>Nodal Points</u>	<u>Elements</u>	
Bottom end plug	1 to 48	1 to 21	(21)
Fuel pellets	49 to 4,376	22 to 2,181	(2,160)
Zircaloy clad	4,367 to 12,384	2,182 to 5,181	(3,000)
Top end plug	12,377 to 12,424	5,182 to 5,202	(21)
Target plate	12,425 to 12,432	5,203	(1)

---

Note: Numbers in parentheses indicate the total number of elements in the component.

#### 4.4.3 The Effect of Irradiation on the Mechanical Properties of Zircaloy-4

Like many other metals, zirconium is strongly influenced by the lattice defects created by fast neutron bombardment. Consequently, the behavior of zircaloy-4 cladding tubing subjected to impact loading cannot be adequately described without taking into account its mechanical properties in the irradiated state. The properties of particular interest in this analysis are yield stresses, ultimate tensile stress, total elongation, modulus of elasticity, and Poisson's ratio.

The effect of irradiation on these properties must be reviewed and assessed for a given clad temperature, neutron dose, and metallurgical condition. For this study, mechanical properties are evaluated at a temperature of 280°C and a fluence (time integral of the particle flux density) of  $2.7 \times 10^{20}$  neutrons/cm<sup>2</sup> (Ref. 24). The more common methods of tube manufacture involve hot extrusion of a hollow billet to a hollow tube, followed by cold reduction with interstage annealing treatments, and final stress relief or recrystallization anneal. The properties of the tube vary according to the amount of residual cold work. Since the 13.1 percent cold work is the most common case, the mechanical properties of zircaloy at this amount of cold work is selected for the present study.

The mechanical properties of irradiated and unirradiated zircaloy are presented in Table 4-3. Because of the scarcity of published data on irradiated zircaloy-4, some of the values (as indicated) are given for zircaloy-2 instead of zircaloy-4. In addition, few researchers have tested irradiated zircaloy-4 fuel cladding under conditions that represent the stressing systems operative in a fuel pin, and few results have been published. Since the difference between the known values for the two alloys is less than 10 percent, and no significant differences have emerged from the recent development work on the two alloys, the use of zircaloy-2 properties for the unknown values is considered to be adequate for this initial analysis.

Investigations have shown that, in general, exposure to neutrons increases ultimate tensile strength and yield strength, and decreases ductility. Furthermore, these effects become more pronounced as the neutron dose increases. In addition, these same characteristic changes occur at all temperatures of interest in this study - room temperature to about 400°C.

The fabrication history, however, has a large effect on the irradiated properties. Irradiating a material is comparable to cold-working it. Both processes increase the strength and

Table 4-3

MECHANICAL PROPERTIES OF ZIRCALOY AT 280°C  
AND 13.1% COLD WORKING

<u>Property</u>	<u>Alloy</u>	<u>Irradiated</u>	<u>Unirradiated</u>	<u>Ref.</u>
Proportional limit, ksi	2	57.7	41.0	24
2% offset yield stress, ksi	2	61.0	47.8	24
Ultimate tensile stress, ksi	2	62.1	48.8	24
Total elongation, %	2	9.0	13.0	24
Density, lb/in. <sup>3</sup>	4	0.237	0.237	25
Modulus of elasticity, ksi	4	14,000	14,000	25
Poisson's ratio	4	0.35	0.35	26,27

decrease the ductility. Specifically, materials that have more than 20 percent cold working prior to irradiation show much smaller increases in their ultimate tensile strength and yield strengths. Kemper and Kelly (Ref. 28) also found that these changes are recoverable and approach the values for the unirradiated materials by annealing for 200 hours at 250°C. However, irradiated materials do not recrystallize during post-irradiation annealing, whereas cold-worked materials will recrystallize if a sufficiently high annealing temperature is used.

#### 4.4.4 Material Modeling for the Fuel Pin

Material properties at a temperature of approximately 300°C for UO<sub>2</sub> and zircaloy cladding were input into this model. At this temperature, UO<sub>2</sub> is nearly brittle, which means that the fracture of UO<sub>2</sub> will take place with a very small or no plastic strain. However, an effective plastic strain equal to 10 percent of yield strain was assumed as the failure strain for UO<sub>2</sub>. This assumption is necessary in order to use the elastic-plastic

failure material model in the computer code employed, and it does not cause a significant deviation from the brittle behavior of  $UO_2$ . At the same temperature (300°C), zircaloy cladding is relatively ductile even after being irradiated. It has a failure (effective plastic) strain of 0.0864, or a total strain of 0.09. In this analysis, after an element fails, it no longer takes tension and the deviatoric stresses, but can still be subjected to compression.

Although zircaloy cladding has a strain-softening characteristic after the initial yielding (Ref. 24), an equivalent bilinear strain hardening relationship was employed to avoid possible numerical instability in the computer analysis. This equivalent strain hardening material was based on the equivalence of energy absorption capacity. Table 4-4 summarizes the material properties used in this model.

Table 4-4  
MATERIAL PROPERTIES OF THE FUEL PIN MODEL

<u>Property at 300°C</u>	<u>UO<sub>2</sub></u>	<u>Zircaloy Cladding</u>
Density, lb/in. <sup>3</sup>	0.372	0.237
Modulus of elasticity, ksi	30,400	14,000
Shear modulus of elasticity, ksi	11,220	5,185
Yield stress, ksi	18.85	50.00
Modulus of strain hardening, ksi	304	140
Yield strain	0.00062	0.00357
Effective plastic strain at failure	0.000062	0.086430
Bulk modulus, ksi	34,940	15,560
Poisson's ratio	0.355	0.350
Ultimate tensile stress, ksi	18.87	62.10

#### 4.4.5 Results of the Analyses

A fuel pin free-falling 30 ft to the target surface reaches a maximum velocity of 527 in./sec. at the point of impact, which was prescribed as the initial condition for the analysis. The analysis was carried out for a duration of 1,000 microseconds.

The deformations of the fuel pellets and zircaloy cladding are shown in Figure 4-8. At 50 microseconds, the fracture of the bottom pellet (height, 0.53 in.) was found. After the failure of the bottom pellet, interaction between the failed pellet and the zircaloy cladding started. At 100 microseconds, the next bottom pellet failed. The interaction between the failed fuel pellet and zircaloy cladding caused the bottom zircaloy clad to expand outward continuously. At 350 microseconds, the first failure of zircaloy occurred at approximately 0.30 to 0.45 in. from the bottom surface of fuel pellet. As time passed, this failure extended downward. At a time 550 microseconds from the beginning of impact, the failure of the zircaloy clad stopped at approximately 0.15 in. from the bottom surface of the fuel pellet. At 800 microseconds, when the impact wave reached the top of the fuel pin, three fuel pellets fractured. When the computation was terminated at 1,000 microseconds, no additional fuel pellet fractured, although the deformation of the fuel pellet and zircaloy cladding continued to increase. The fractured portion of the fuel pellets amounted to about 1.325 in., or less than 1 percent of the total height of the fuel pellets. Table 4-5 summarizes the accumulated effective plastic strains at critical locations.

Table 4-5

## ACCUMULATED EFFECTIVE PLASTIC STRAINS

<u>Component</u>	<u>Location</u> (from the bottom of fuel pin)	<u>Accumulated Effective Plastic Strain</u>
Bottom end plug	Middle thickness	Ductile failure
Fuel pellet	0.69-2.01 in.	Brittle failure
Zircaloy cladding	0.69-0.84	0.0701
	0.84-1.14	Ductile failure
	1.14-1.29	0.0845
	1.29-1.44	0.0785
	1.44-1.59	0.0605

## 5.0 FUEL PELLET PULVERIZATION

### 5.1 Introduction

Brittle materials are those that fracture without plastic deformation when subjected to tensile strain above the elastic limit. Common glasses, ceramics, and  $UO_2$  are brittle materials by this definition, but common metals are not. The impact-fracture behavior of selected brittle materials was examined in a study conducted at Argonne National Laboratory (ANL) in 1979-1981 (Refs. 29 and 30). Although a variety of materials and a range of impact configurations and conditions were used, the generalized results found cannot be said to have received sufficient empirical support to establish their generality as theory. Nevertheless, the basic principles of physical mechanics, the theory of elasticity, material science, and small-particle statistics have been combined to provide a useful analytical tool for research in a very difficult area, namely impact fracture with its noncontinuum, nonequilibrium mechanics and thermodynamically irreversible rate processes.

The ANL analysis were based on the well-established theory of elasticity (Ref. 31), on the state-of-the-art of glass science (Ref. 32), and on energy-surface area correlations established experimentally for small specimens of glass and quartz (Ref. 33). The application of the lognormal probability function to describe the size distribution of fracture particulates followed the state-of-the-art of small-particle statistics (Ref. 29). Details and conclusions of the ANL experimental tests on selected materials have been reported previously, by Mecham et al. (Ref. 29) and Jardine et al. (Ref. 30).

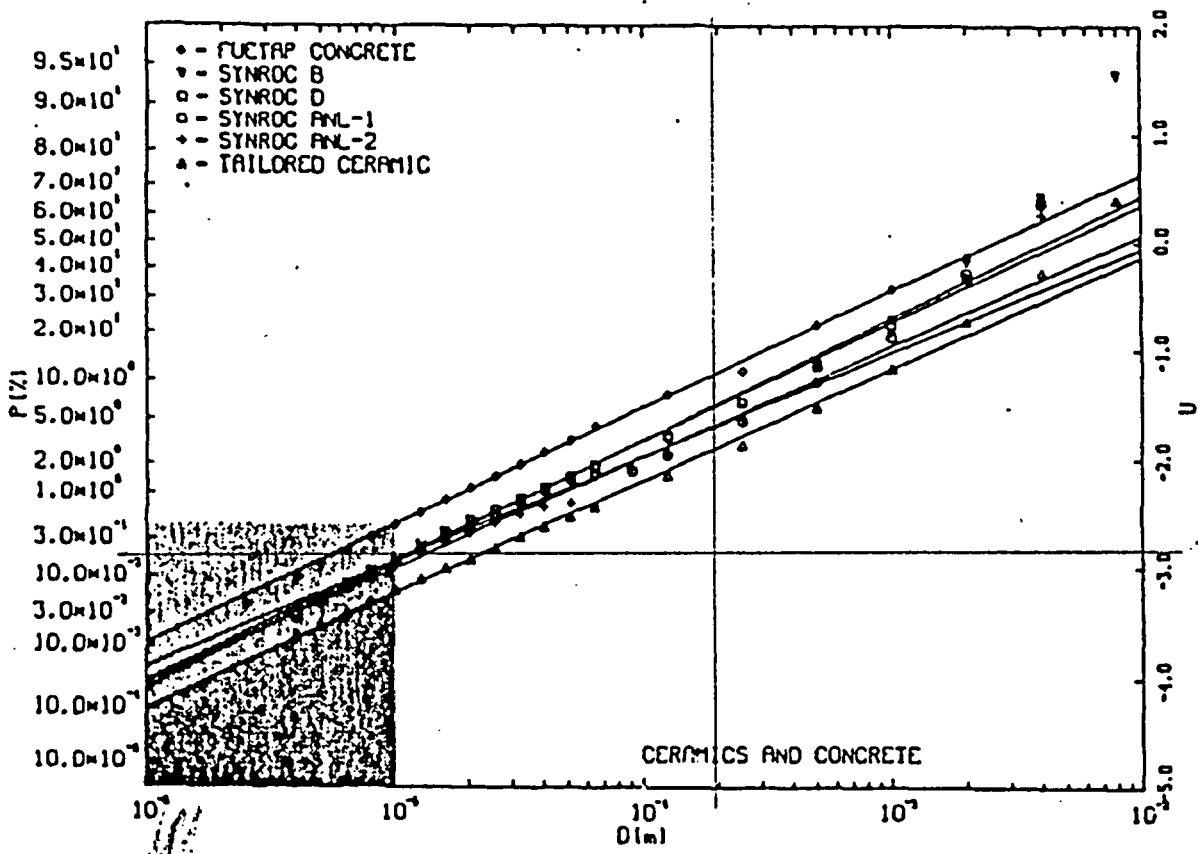
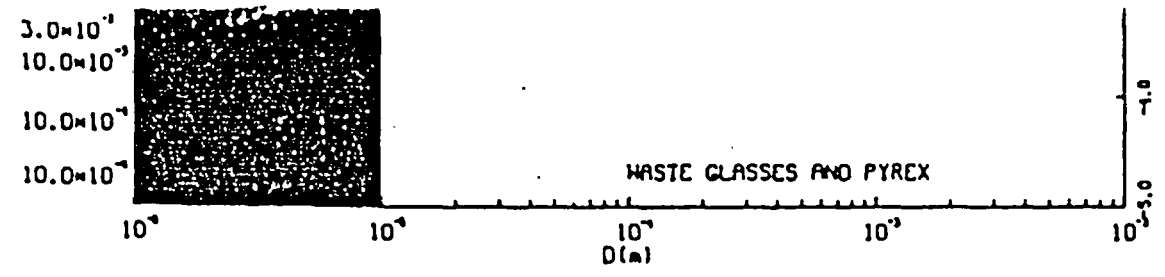
### 5.2 Impact Fracture of Brittle Materials

In the ANL studies, a literature review was conducted as a preliminary phase of a study of the impact fracture of brittle

materials (Ref. 29). The principal conclusions of this review were the following:

- o If sufficiently high levels of elastic strain energy per unit volume of materials (energy density) can be developed within brittle material by the application of an external force, the material disintegrates into particles of a range of sizes, including submicron particles. This happens for both slowly and rapidly applied forces and for tensile and compressive forces.
- o This fracture behavior is consistent with current knowledge of fracture mechanics and with observed rates of crack propagation, as well as with correlations of fracture surface area with energy dissipated in the brittle material.
- o Lognormal statistics have been developed for describing fracture particulates, and the empirical lognormal size distributions provide a general model of the impact-fracture process (Refs. 34 and 35).

A preliminary series of drop-weight impact tests of representative brittle materials was made (Ref. 29). Cylindrical specimens (approximately 25 mm x 25 mm) were impacted diametrically in a bellows-sealed impact chamber by a falling 10 kg steel bar, and the resulting particle size distributions were measured by sieving the Coulter counter analysis (down to about a 5-micron size). The materials tested included: Pyrex glass, Macor glass ceramic, sintered  $UO_2$  ceramic, and fused quartz (vitreous silica). Three natural materials were also tested: crystalline quartz, nepheline syenite, and sandstone. All results showed that the fracture particulate proper, which included all particles of respirable size (i.e., diameters less than 10 microns), and which contained more than about 90 percent of the total surface area, had a straight-line size distribution when plotted on lognormal graphical coordinates as shown in Figure 5-1 (Ref. 30).



1.96E-4

Figure 5-1

Computer Regression Analysis Plots of P(%), the Cumulative Lognormal Mass Distributions (in mass percent of initial specimen mass) of Fragments vs D(m), the Measured Fragment Diameters from 10 J/cm<sup>3</sup> Impact Tests of (1) Glasses (Upper Plot) and (2) Crystalline Ceramic and Concrete Simulated Waste Forms (Lower Plot). The shaded areas correspond to potentially respirable particles (i.e., <u>10 μm</u>).

0.000196 = 0.0196%  
1.96E-2

### 5.3 Empirical Descriptions of Fracture Particulates

Empirical characterization of the size distributions of particles produced from brittle material by various crushing processes has led small-particle statisticians to extensive application of the lognormal probability function, e.g., Herdan (Ref. 34), although this lead has not been much followed by experimenters. The applicability of the lognormal mathematics to characterization of particulates is very extensive. Of course, the utility of using a lognormal analysis rests not on theoretical, but on empirical grounds. Size-distribution measurements give data points that plot as an approximately straight line on lognormal graphical coordinates.

### 5.4 Correlation of Impact Energy and Fracture Surface Area

The thermodynamic (reversible) free energy of surface formation in a typical brittle material is the order of  $1 \text{ J/m}^2$  (Ref. 33). In practical impacts, the energy consumption is much higher per unit of surface formed. In a systematic study of the energy-surface correlation conducted at the University of Minnesota in 1962, an impact calorimeter was used to make an energy balance for the fracture of small Pyrex and quartz (vitreous and crystalline) specimens over a wide range of energy input. The particle sizes were not measured, but the total particulate surface area was measured by the BET gas-adsorption method. The principal equation investigation was

$$\epsilon W_o = \gamma_f S_n \quad (1)$$

where  $W_o$  was the energy input,  $\epsilon$  was the fraction of input kinetic energy actually dissipated in the brittle material (measured with the calorimeter),  $S_n$  was the measured total fracture surface area, and  $\gamma_f$  was the material fracture strength calculated from the equation. The input energy density

(energy per unit volume of material) varied over a factor of 20 in these tests, but the value of the impact-strength property  $\gamma_f$  was constant (within about 5 percent) at a value of  $77 \text{ J/m}^2$ . The value of  $c$  was measured in the range of 0.5 to 0.95 in these tests (Ref. 33). In the ANL impact tests, different values of  $c$  could have occurred, but the basic energy-surface correlation was corroborated in the ANL work.

### 5.5 Surface Areas and Shape Factors

Although the particles produced by impact fracture are very irregular, the irregularity (as observed with the microscope and electron microscope) is definitely limited by physical conditions. There are, for instance, no extremely long needle-shaped particles nor any very thin plate-shaped particles. A statistical mean surface/volume ratio can be used to describe the actual particles. For a given particle diameter  $D$  (however measured), there is both a mean volume and a mean surface, each of which can be expressed mathematically as a shape factor. From available empirical data, it appears that these shape factors are uniform over the range of size of the fracture particulate, although different materials may have somewhat different shape factors. The shape factor of practical interest is  $\alpha$ : the surface area/volume ratio for the lognormal fracture particulate as a whole.

One of the mathematical properties of the lognormal particle statistics is that, once the mean diameter,  $D_g$ , and the standard deviation,  $\sigma_g$  for the volume distribution are known, the surface-area distribution can be calculated.

For an ideal (complete) lognormal distribution ( $0 \leq D \leq \infty$ ), there is a mathematical relation for the ratio of the total surface area,  $S_n$ , and the total volume,  $V_n$  of the particles

$$\frac{S_n}{V_n} = \frac{\alpha \sigma_g}{D_g} \frac{0.15 \ln \sigma_g}{1} \quad (2)$$

where  $\alpha$  is the overall surface/volume shape factor. If Equations (1) and (2) are combined

$$\frac{\epsilon}{\gamma_f} \frac{W_o}{V_n} = \frac{S_n}{V_n} = \frac{\alpha \sigma_g^{0.15} \ln \sigma_g}{D_g} \quad (3)$$

Now, if the input energy,  $W_o$ , specimen volume,  $V_n$ , particulate surface area (by BET method)  $S_n$ , and  $D_g$  and  $\alpha$  (by sieving) are measured both the shape factor,  $\alpha$ , and the combined strength parameter ( $\gamma_f/\epsilon$ ) can be calculated. This gives a complete characterization of the results of fracture, since the size fractions and surface areas of the particulate are determined for the full range of particle diameters.

#### 5.6 Correlation of Fracture Parameters with ANL Input Energy Density

In Equation (3) above, the fracture surface/volume ratio,  $S_n/V_n$ , is proportional to the impact energy density,  $W_o/V_n$ ; the proportionality constants are the lognormal fracture parameters previously identified. The utility of the impact-characterization method described here depends on being able to correlate the fracture parameters with impact conditions and material properties. Preliminary correlations were presented in Table 5-1, which summarizes the results of five diametrical impact tests of Pyrex specimens (38 mm dia. x 68 mm long cylinder, Ref. 36). Impact energy densities varied 20-fold. In addition, the correlation of the respirable sizes (less than 10 microns) versus the energy density was compiled in this study. These results are shown in Figure 5-2 and Table 5-2. Of the parameters listed, the mean diameter,  $D_g$ , was inversely proportional to energy density; the others,  $\sigma_g$ ,  $\alpha$ ,  $\alpha_f/\epsilon$ , etc., were approximately independent of energy density. From the percentage range indicated, the accuracy of these correlations was within about a factor of 2. A similar accuracy was observed for the respirable fraction, the volume fraction of particles with diameters less than 10 microns, which was directly proportional to

retains its integrity. It should be noted that this conclusion was based on analyses that were conducted using very limited resources. Further studies are recommended to learn more about the dynamic response of the container to the potential various impacts. These recommendations are given in Subsection 6.2.2.

#### 6.2.2 Recommendations

In future studies of the limiting drop height of the container, the following should be investigated:

- o The effect of impact orientation, especially the impact on the pintle of the container
- o The effect of total container weight on the limiting drop height
- o The effect of interactions between the fuel assemblies and interactions between fuel assemblies and the container on the limiting drop height.
- o The effects of container impact on sharp objects and various target conditions
- o Confirmatory laboratory or full-scale testing.

#### 6.3 Drop of Fuel Assembly and Spent Fuel Pulverization

##### 6.3.1 Conclusions

A 30 ft drop analysis of a typical Westinghouse 17 x 17 PWR fuel assembly was performed using hand calculations to estimate the energy absorption by various parts of the fuel assembly. A finite-element impact analysis by DYNA3D was performed for a separated individual fuel pin with a 30 ft drop height. As a result of this analysis, the following conclusions were drawn:

- 
- o The friction between fuel pins and the grid spacers dissipates only a small amount of the impact energy, approximately equal to 3 percent of the total kinetic energy imparted to the fuel pins.
  - o The bottom 1.3 in. of fuel pellets (which is less than 1 percent of the total volume) fractures.
  - o The zircaloy cladding fails in the region (0.15 to 0.45 in from the bottom of fuel pellet) where the fractured fuel pellet expanded radially.
  - o There is no failure in the bottom end-plug of the fuel pin.

#### 6.3.2 Recommendations

Further studies on the effect of impact on fuel assemblies and fuel pins are recommended. These studies should investigate the effect of lateral buckling on the failure of fuel pellets and the zircaloy cladding. Correlations of the initial small-scale ANL impact tests with the individual fuel pin finite-element modeling results should be attempted, and recommendations for future confirmation laboratory and fuel-scale testing should be made on the basis of this modeling. A simplified finite-element model can be created for the fuel assembly. A finite-element impact analysis, instead of the (oversimplified) hand calculations by the energy balance method, may be carried out to determine the energy absorption of the bottom nozzle so that the effect of the bottom nozzle on the dynamic response of fuel pins can be accounted for more realistically. The effects of nonperpendicular impact and impacts on various target conditions should also be investigated.